On the kinetic modeling of collisional effects relevant for non-stationary magnetoplasmadynamic thrusters

IEPC-2011-307

Presented at the 32nd International Electric Propulsion Conference,
Wiesbaden, Germany
September 11–15, 2011

Dejan Petkow*
ESA-ESTEC, Noordwijk, 2200 AG, The Netherlands

and

Georg Herdrich† and Stefanos Fasoulas‡
Institute of Space Systems, Universität Stuttgart, Stuttgart, 70569, Germany

and

Monika Auweter-Kurtz§
German Aerospace Academy ASA, 71304, Böblingen, Germany

Within the framework of a fully kinetic 3D plasma particle code, a Direct Simulation Monte Carlo (DSMC) module is under development at the Institute of Space Systems. For the complete discharge simulation of a non-stationary magnetoplasmadynamic thruster we have developed an improved DSMC model for collisional short range interactions: A high fidelity collision and reaction evaluation model which is based on energy dependent cross section data only. This work was accompanied by the implementation of Monte Carlo Coulomb Collision (MCCC) solver for the treatment of Coulomb collisions which naturally a long range interactions.

Cross section data are based on Carbon due to the relevance of Polytetrafluorethylen as prominent propellant in non-stationary magnetoplasmadynamic thrusters. Initial assumptions (fully dissociated and partially ionized propellant material) reduced the number of considerable species and interactions. Here we focus on electron - heavy particle interactions which are elastic scattering (including polarization), collisional excitation, ionization, de-excitation, and non-radiative recombination.

The verification procedure in case of DSMC is based on the reproduction of rate coefficients in the range of $20.000 - 200.000\ K$. Verification was successful for ionization, excitation and recombination. Main problems for future works concern the improvement of the Coulomb collision cross section model as well as the numerical generation of a reference for the collisional de-excitation process.

The MCCC solver was verified on basis of analytical solutions for an electron shot into an ion and into an electron cloud.

*Research Fellow, Advanced Concepts Team, dejan.petkow@esa.int.

†Professor, Head of Electric Propulsion and Re-entry Technology, Space Transportation Technology, herdrich@irs.uni-stuttgart.de.

‡Professor, Head of Department, Space Transportation Technology, fasoulas@irs.uni-stuttgart.de.

§Professor, Director of German Aerospace Academy, m.auweter-kurtz@german-asa.de.

Nomenclature

0 = ground state, initial state
$\tilde{A}...\tilde{E}$ = coefficients
A = function
A_k = coefficients of fit function
a_0 = Bohr radius
dex = subscript electron induced de-excitaion
c = subscript collision
c_0 = vacuum speed of light
cou = subscript Coulomb scattering
D = subscript differential
E = energy, background electron species
ela = subscript elastic scattering
exc = subscript electron excitation
e = elementary charge, subscript electron species
f = distribution function
F = probability density function
$\vec{F}$ = force
$\vec{g}, g$ = relative velocity, degeneracy
G = number of single excitation transitions
h = Planck's constant, subscript heavy particle
i = interaction index, counter, subscript ion species
ion = subscript electron impact ionization
j = index state of charge
k_B = Boltzmann's constant
m = particle mass, index initial excitation state
m_r = reduced mass
n = particle (number) density, index final excitation state
N = number of single scattering events, number of particles
P = probability
$phion$ = subscript photo ionization
Q = number of particle pairs
R = equally distributed random number $\in [0, 1]$
rad = subscript radiative recombination
rec = subscript non-radiative recombination
T = temperature, subscript total
$t, \hat{t}$ = time (normalized)
$\vec{x}$ = position vector, spatial information
$\vec{v},\ \hat{v}$ = velocity vector, normalized velocity
V_{cell} = cell volume
X = non-dimensional energy
Z = charge number

α = species index (test particle), relative polarizability
β = species index (background particle)
δ = Kronecker symbol
ϵ = azimuthal scattering angle
λ_D = Debye length
ν = photon frequency, relaxation frequency
ε_0 = dielectric constant
σ = (integral) cross section
τ = isotropy parameter
χ_N = cumulative scattering angle after N collisions
Ψ = mole fraction
Ω = collision strength
$\triangle t$ = time step size
$\ln \Lambda$ = Coulomb logarithm
$||$ = parallel
$\perp$ = perpendicular

I. Introduction

PRESENTLY, a highly non-stationary plasma thruster (iMPD)[1] is under development at the Institute of Space Systems (IRS), see Fig. 1. Pulsed thrust generation is based on several steps: The solid propellant Polytetrafluorethylen (PTFE) which is positioned between the two electrodes is partially ionized by an initial discharge. The resulting electron current induces a magnetic field which interacts with the charged particles. Light and fast electrons experience a much stronger Lorentz force than heavy and slow ions which would lead to charge separation. Ions are mainly accelerated by strong electric fields and decelerated by collisions with neutrals. The oscillation of the discharge current leads to more than one discharge and further coupling processes between the external and the plasma circuit. All of these processes make the thrust generation a very complex and barely understood phenomenon even though such thrusters have been applied for decades.

A. Problem Description

Numerically, plasma flows can be described either by continuum or particle methods, depending on the occurring gradients and time scales. The iMPD thruster stores a capacitor bank energy of about $70J$ at roughly $1300V$. During a discharge this energy is partially transferred to the plasma. If one assumes a coupling efficiency of 20%, then a discharge duration of about $15\mu s$ leads to very high mean pulse powers ($\sim 1MW$) and, correspondingly, to strong gradients and deviations from any equilibrium distribution function as the ablated mass bit is of the order of $50\mu g$. Therefore, the application of MHD codes, which naturally need assumptions for the energy distribution and its possible deviation from the equilibrium, is generally questionable. However, scientific efforts in the field of extended hydrodynamics[2,3] have not been very fruitful so far.[4]

Although one can find published work on particle based simulations of pulsed plasma thrusters,[5–7] each work is based on at least one of the following assumptions or simplifications:

- Particle code is not fully kinetic but hybrid, i.e. the electrons are modeled as a fluid.
- Only the plume is simulated, not the complete discharge.
- Time dependent field effects are neglected by use of Poisson equation.
- Simulation domain is reduced by assuming axi-symmetricity.

Typical consequence of making those simplifications is the observation that there is a considerable mismatch between the measurement and the simulation.[6] Especially the creation of hot spots due to the low temperature of the cathode makes each coaxial thruster a full 3D problem.[7]

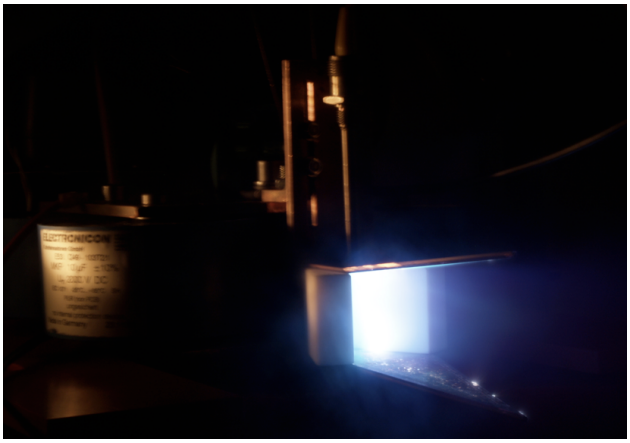

Figure 1. Discharge of the iMPD thruster ADD SIMPLEX.[1]

B. Solution Strategy

A cooperation between IRS (Institute of Space Systems, Universitt Stuttgart), IAG (Institute of Aerodynamics and Gas Dynamics, Universitt Stuttgart), ASE (Applied Supercomputing in Engineeering, German Research School for Simulation Sciences), and IHM (Institute or Pulsed Power and Microwave Technology, Karlsruher Institut fr Technologie) is working on the modeling of highly rarefied and transient plasma flows which typically occur during the initial discharge and acceleration phase of (and inside of) an iMPD thruster.

The governing equation for this problem is the Boltzmann equation

$$\frac{\partial f_\alpha}{\partial t} + \vec{v_\alpha}\frac{\partial f_\alpha}{\partial \vec{x}} + \frac{\vec{F}_\alpha}{m_\alpha}\frac{\partial f_\alpha}{\partial \vec{v}_\alpha} = \int_{-\infty}^{\infty}\int_0^{4\pi} \left[f(\vec{v}'_\alpha)f(\vec{v}'_\beta) - f(\vec{v}_\alpha)f(\vec{v}_\beta)\right] g\sigma_D \mathrm{d}\Omega \mathrm{d}\vec{v}. \tag{1}$$

which describes the evolution of the velocity distribution function $f_\alpha = f(v_\alpha)$ of species α scattered by a background species β. The left side of Eq. (1) describes the change of f_α over time t, the dependence of f_α on spatial inhomogenities, and the change of f_α as a consequence of external forces F_α accelerating the particles with the mass m_α. Those forces a typically electrostatic and Lorentz forces. The right side of Eq. (1) describes the change of f_α due to inter-particle collisions. Collisions are described by the collision cross section σ_D which depends on the relative velocity g between both particles. Post-collisional quantities are primed.

The mathematical treatment of the Boltzmann equation is extremely difficult.[8–10] The common approach is to split Eq. (1) in corresponding domains such that the dominating physical processes are defined by certain temporal and spatial scales.

Within that project a scheme for approximately solving the full Boltzmann equation for rarefied, non-continuum plasma flows is under development: A PIC (Particle In Cell) solver is used for the non-stationary Maxwell-Vlasov equation[11] and a DSMC solver for the binary collision Boltzmann equation. Moreover, Nanbu's Fokker Planck solver[12] for the treatment of Coulomb collisions was implemented as well as a new self-consistent Fokker Planck solver on basis of an equivalent stochastic differential equation (SDE).[13] In this report we focus on two code extensions:

1. The DSMC module which deals with collisional *short* range interactions between electrons and heavy particles.

2. The MCCC module which deals with collisional *long* range interactions between charged particles.

In section II we present the DSMC approach and give detailed information on the implemented cross sections and the verification process. Section III gives a brief introduction to the MCCC theory and the verification methodology. Concluding remarks can be found in section IV together with a brief summary and recommendations for future activities.

II. DSMC Model, Verification, and Discussion

Given the constraints in the introductory section it seems to be required - or at least justified - to avoid simplifying assumptions as much as possible. Regarding DSMC it is concluded that classical cross section models like Variable Hard Sphere[14] or Generalized Hard Sphere[15] are inappropriate for the modeling of pulsed plasma thrusters as they incorporate quantities which are defined at equilibrium, namely viscosity and diffusion. The obtained cross sections are energy dependent but scale with a temperature respective behavior. Therefore, the total (integral) cross section

$$\sigma_T(E) = \sum_i \sigma_i(E) \tag{2}$$

as a sum over i interaction types is introduced. The energy equals the collision energy $E_c = m_r g^2/2$ where m_r is the reduced mass of the colliding particles. For the sake of consistency, the interaction type dependent cross section models should be as accurate as possible in the sense that no macroscopic quantities are implied in their derivation processes.

In our DSMC model, collision evaluation is treated on basis of the Natural Sample Size (NSS) method.[16] The resulting collision probability equals

$$P_c = \frac{n_\alpha n_\beta}{1+\delta_{\alpha\beta}} \frac{V_{cell}\triangle t}{Q_{\alpha\beta}} \sigma_T g \tag{3}$$

where n, , V_{cell}, $\triangle t$, and $Q_{\alpha\beta}$ represent particle densities, cell volume, time step size, and the number of possible collision pairs. The Kronecker symbol $\delta_{\alpha\beta}$ accounts for possible double counts.

Contrary to the Constraint Probability (CP) method which is implemented in most published DSMC codes the NSS method can be considered as a two step method: In a first loop *all* particle pairs are evaluated. Then, in a second loop all colliding pairs are evaluated concerning the concrete interaction type. The individual reaction probabilities result from

$$P_i = \frac{\sigma_i}{\sigma_T}. \tag{4}$$

On a first glimpse this procedure sounds disadvantageous with respect to CP. However, NSS allows a much more elegant way to consider recombination reactions where in advance a third particle needs to be stored. Also, NSS inherently prohibits a collision number which is larger than the number of available particle pairs. One drawback inherent to NSS is the control of the maximum collision probability (via time step size adaptation) which in CP never exceeds unity.

A. Particle pair types

Assuming a fully dissociated and partially ionized PTFE plasma one has to consider Carbon and Fluorine and their charged and excited derivatives. However, in case of Fluorine the available data are very scarce, hence the overall model approach is presented here on basis of Carbon. The considered species are C, C^+, C^{2+}, C^{3+}, C^*, C^{*+}, C^{*2+}, C^{*3+}, and e. This implies the following relevant particle pair types: *electron - atom*, *electron - excited atom*, *electron - ground state atomic ion*, and *electron - excited atomic ion*. Interactions of the types *ion - ion* and *neutral - ion* play an important role in the plume area but are neglected here as focus is on the discharge chamber where the electron induced processes dominate.

In order to provide accurate cross sections each pair type may require an individual cross section model.

For the sake of flexibility, a data scheme was developed and implemented which allows a very efficient correlation between the current particle pair and the implemented cross section models, see Table 1 in the Appendix. Therein, A, M, I, M^+, A^*, I^*, M^*, and M^{*+} represent the ground state atom, the ground state (diatomic) molecule, the ground state atomic ion, the electronically excited atom, and so forth. In our code, each pair can be assigned to its model by simply adding both InterID values in order to obtain an integer value for a bijective *select case* based assignment structure. Generally, this assignment method allows not only specific and individual cross section modeling but also a quick extension of the set of allowed particle types. Given the above listed Carbon species, the following pair types are obtained:

$A - e$: When an electron collides with a ground state atom, three possible interactions may occur: elastic scattering, excitation and ionization. Therefore, the total collision cross section is

$$\sigma_T = \sigma_{ela} + \sigma_{exc} + \sigma_{ion}. \tag{5}$$

$A^* - e$: In this case the resulting σ_T is a bit more complex because collisional de-excitation may occur:

$$\sigma_T = \sigma_{ela} + \sigma_{exc} + \sigma_{ion} + \sigma_{dex}. \tag{6}$$

$I - e$: Although DSMC is naturally not well applicable to elastic charge-charge interactions, reliability of the probability computation is improved if as many of the relevant effects as possible are considered in the denominator of Eq. (4). Hence, the Coulomb scattering is represented by a corresponding cross section. Note, that the radiative recombination process represented by σ_{rad} is concurring to the non-radiative (i.e. three body) recombination process. Although radiation is not computed explicitly its consideration improves the computation reliability. Now, one gets

$$\sigma_T = \sigma_{cou} + \sigma_{exc} + \sigma_{ion} + \sigma_{rec} + \sigma_{rad}. \tag{7}$$

$I^* - e$: In case of an electron impact a de-excitation process may occur additionally:

$$\sigma_T = \sigma_{cou} + \sigma_{exc} + \sigma_{ion} + \sigma_{rec} + \sigma_{rad} + \sigma_{dex}. \tag{8}$$

In the following paragraphs the different models to describe the various cross sections are depicted.

B. Cross section models

In the following section the implemented cross sections are summarized.

1. Elastic electron scattering

For elastic electron scattering, a model for high electron energy is applied:[17]

$$\sigma_{ela}(E_c) = \sqrt{\frac{\pi\alpha e^2}{2\varepsilon_0 E_c}}. \tag{9}$$

In Eq. (9) α is the polarizability of the target atom, in case of Carbon[18] $\alpha = 11.46a_0^3$; a_0, ε_0, and e are the Bohr radius, the dielectric constant, and the elementary charge. This model was derived applying a high energy approximation. Therefore, its validity is generally restricted to $E_c >> R_y a_0^3/\alpha \approx 1.187eV$.

2. Electron impact excitation

The electron excitation cross section equals the sum over all G single cross sections for the transitions from the initial excitation state m to the final state n:

$$\sigma_{exc} = \sum_{i=1}^{G} \sigma_{exc,mn}. \tag{10}$$

This is justified since each single transition process is possible and, therefore, is treated as a separate occurrence within this probability approach.

Electron impact excitation is modeled on basis the work of Suno and Kato.[19] They compiled and analyzed cross section data which were not older than 1985. For older data they used the given references. Generally, experimental data were preferred in comparison with numerical/theoretical data in order to identify appropriate fit functions. In case of theoretical references, Close-Coupling and R-Matrix computations[20] were favored at low energies. At high energies Distorted-Wave and Coulomb-Born method[21] were preferred. In the following the fitting procedure of given data sets is described. All coefficients and quantities are listed in the publication of Suno and Kato.[19]

The fitted quantity is not the cross section itself but the related non-dimensional collision strength Ω_{mn} with m and n describing the initial and the final state. The excitation cross section is defined as

$$\sigma_{exc,mn} = 1.1969 \cdot 10^{-19} \frac{\Omega_{mn}^{I,II}}{g_m E_c}, \tag{11}$$

where g_m is the degeneracy of the state m. Applying the collision energy in $[eV]$ yields a cross section in $[m^2]$. Moreover, introducing the non-dimensional energy

$$X = \frac{E_c}{E_{mn}} \quad \text{with} \quad X > 1 \tag{12}$$

with E_{mn} representing the energy gap between the states, two different fit functions are identified: Type I has the following structure:

$$\Omega_{mn}^{I}(X) = \tilde{A} + \frac{\tilde{B}}{X} + \frac{\tilde{C}}{X^2} + \frac{\tilde{D}}{X^3} + \tilde{E}\ln X. \tag{13}$$

Therein, $\tilde{A}...\tilde{E}$ are known and published coefficients.[19] In cases where this fit function type was not suitable in order get a high fidelity approximation, a second type was introduced:

$$\Omega_{mn}^{II}(X) = \frac{\tilde{A}}{X^2} + \tilde{B}e^{-\tilde{F}X} + \tilde{C}e^{-2\tilde{F}X} + \tilde{D}e^{-3\tilde{F}X} + \tilde{E}e^{-4\tilde{F}X}. \tag{14}$$

This type contains the additional coefficient $\tilde{F}$.

Some original data sets were given as rate coefficients. In such cases, the collision strength was integrated and the rate coefficient approximated. For details please refer to the relevant reference[19] which, of course, contains information on the assignment between the applied fit function to the species pairing as well as all fit function coefficients.

3. Electron impact ionization

Suno and Kato[19] used similar approaches to find high fidelity fit functions for the ionization cross section

$$\sigma_{ion}(E_c) = \frac{10^{-17}}{E_{ion}E_c}\left[A_1 \ln\left(\frac{E_c}{E_{ion}}\right) + \sum_{k=2}^{N} A_k \left(1 - \frac{E_{ion}}{E_c}\right)^{k-1}\right] \tag{15}$$

where E_{ion} is the species dependent ionization energy. All energies are in $[eV]$ and the coefficients A_k can be found in the main reference. The authors give approximation errors with respect to the original data sets which are in the range of 0.1% to 1.46%.

4. Collisional electron de-excitation

For the typical backward reactions de-excitation and recombination the *Detailed Balancing* principle is applied which allows to use a proportionality relation

$$\sigma_m g_m \sim \sigma_n g_n. \tag{16}$$

between the cross section of the forward and backward reaction. Applying this principle to the electron impact excitation yields

$$\sigma_{dex}(m, n, E_c) = \frac{g_n}{g_m}\frac{E_c}{E_c - E_{mn}}\sigma_{exc}(n, m, E_c). \tag{17}$$

5. Collisional electron recombination

Again, the *Detailed Balancing* principle is applied and leads to

$$\sigma_{rec}(0, E_c) = \frac{g^{(j-1)+}}{2g_0^{j+}}\left(\frac{h^2}{2\pi m_e k_B T_e}\right)^{3/2} n_e \frac{E_c}{E_c - E_{ion,0}}\sigma_{ion}(0, E_c) \tag{18}$$

with j, h, and k_B describing the ion's charge state, Planck's constant, and Boltzmann's constant. This expression implies that the recombination is always to the ground state as $\sigma_{ion}(0, E_c)$ is used. However, the approach generally allows to derive a formulation for the recombination to an excited state. Note, Eq. (18) demands the electron temperature which is a direct consequence of this approach[22] as for free electrons the energy is assumed to be vanishing.

6. Radiative electron recombination

The *Detailed Balancing* principle is again applied in order to derive the photo-recombination cross section. So far, photons are not considered in the overall particle approach. However, the radiative recombination process concurs with the non-radiative process since the only relevant difference is the availability of a second electron in the vicinity of the ion. Taking into account the statistical nature of DSMC as well as the particle discretization one can only extract an information on the probability for each of these two processes which is sufficient. The resulting formulation for the radiative recombination cross section

$$\sigma_{rad}(0, E_c) = \frac{g^{(j-1)+}}{2g_0^{j+}}\frac{E_c^2}{m_e c_0^2}\frac{1}{E_c - E_{ion,0}}\sigma_{phion}(0, \nu) \tag{19}$$

with c_0 being the vacuum speed of light and $E_c = h\nu$ with ν being the photon frequency necessary for the ionization process. Therefore, an available Fortran code for the computation of photo-ionization cross sections σ_{phion} on basis of the R-Matrix method[17,18,23] was implemented. The code was written in the frame of the *Opacity Project*[24] and contains approximations for a huge number of species including Carbon.

7. Coulomb collision

Since a Fokker Planck solver for the Coulomb collisions is used, a simplified expression for the total (integral) Coulomb collision cross section was implemented. The DSMC based treatment of a Coulomb collision introduces the highest uncertainty in the collisional modeling. It is well known that σ_{cou} diverges due

to the infinity if the underlying electrostatic potential function. By introducing some simplifications in the computation of σ_{cou} two approaches have been being established: In the integration of the differential Coulomb collision cross section one can define either a minimal scattering angle or a maximal interaction range which is regularly identified as the Debye length

$$\lambda_D = \frac{e^2|Z_\alpha Z_\beta|}{4\pi\varepsilon_0 m_r \langle g_{\alpha\beta}^2\rangle}\Lambda_{\alpha\beta}, \tag{20}$$

where Z is the charge number and $\langle g_{\alpha\beta}^2\rangle$ is the mean square of the relative velocity. Following Jahn[25] a typical value for the Coulomb logarithm in electric propulsion systems is $\ln\Lambda_{\alpha\beta} \approx 10$. Given that, and with the definition $\sigma_{cou} = \pi\lambda_D^2$ one yields the following simplified expression with the collision energy E_c in $[eV]$:

$$\sigma_{cou} \approx 6.5 \cdot 10^{-17}\frac{Z_i^2}{E_c^2}. \tag{21}$$

C. Verification and Discussion

Reservoir simulations were performed in order to verify the correct implementation of the model approach and of the cross section data on basis of rate coefficients which are independent of the chosen system state. In many cases rate coefficients are given analytically as Arrhenius equation. However, sometimes these quantities are not available, hence numerical tool was developed for the generation of the missed references. The rate coefficient $\langle\sigma g\rangle$ is the energy averaged product of a cross section and the relative velocity between both particles,

$$\langle\sigma_i(E_c)g\rangle = \int_{-\infty}^{\infty}\sigma_i(E_c)gf(g)\mathrm{d}g. \tag{22}$$

In Eq. (23), $f(g)$ is the well known Maxwellian distribution function of the relative velocity g. Since we consider only electron induced processes and, therefore, $E_c \sim m_r g^2 \approx m_e v_e^2$, the equation to be integrated numerically reduces to

$$\langle\sigma_i(E_c)v_e\rangle = \frac{4}{\sqrt{2\pi m_e(k_B T_e)^3}}\int_0^{\infty}\sigma_i(E_c)E_c\exp\left(-\frac{E_c}{k_B T_e}\right)\mathrm{d}E. \tag{23}$$

For the DSMC reservoir simulation a non-geometric cell was initialized with particles according to a predefined energy state, see Table 2 in the Appendix. During each time step particle pairs are chosen randomly and evaluated with respect to possible reactive and non-reactive interactions. The evaluation is realized by only counting the interaction events as such. Given a defined iteration number computation was repeated and counts were averaged in order to reduce inherent statistical fluctuations.

D. Collision and reaction evaluation

1. Collision

The simulation results in case of (e, C) collisions are depicted in Fig. 2. The match can be considered as very good in the complete temperature range. Maximum relative deviation from the reference is at minimum temperature and equals 22.6%. At maximum temperature the relative deviation is about 22.2%. Between these temperatures the relative deviation approaches even zero.

2. Ionization

The results of the ionization evaluation are depicted in Fig. 3 and Fig. 4. The matching is visibly worse than in the pure collision case. For the ionization of ground-state neutrals represented by Fig. 3 the maximum relative deviation is at T_{max} and reaches 45.7%. The lowest relative deviation approaches 29.4% at T_{min}. Very similar results are obtained for the ionization of ground-state ions, depicted in Fig. 4. Both results can be explained by the fact that the ionization cross sections were taken from the work of Suno and Kato,[19] the rate coefficients was taken from Voronov.[26]

In case of (e, C^+) the ionization starts at higher temperatures. The gap between simulation and reference decreases with increasing temperature. The result is also influenced by the use of σ_{cou} in the denominator

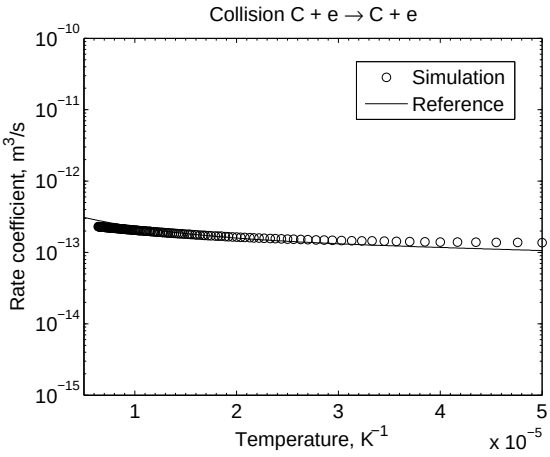

Figure 2. The simulated (e, C) collision rate coefficient in comparison with the reference (Eq. (23)).

of Eq. (4). As mentioned earlier, the Coulomb collision cross section is not suitable for the DSMC modeling of binary collisions. On basis of the presented model approach one gets rate coefficients which show a considerable deviation from the reference since in such a case σ_{cou} is not only in the denominator, but also in the numerator of Eq. (4). Simultaneously, the Coulomb cross section implemented here contains a crude approximation proposed by Jahn.[25] Therefore, additional influence of the result is not surprising even when the uncertainty of σ_{cou} is smeared in σ_T.

Another observation affects the statistical property of DSMC. In Fig. 4 one can see statistical scattering at lower temperatures. This trend is also observable in the (here not presented) plot of the (e, C^{2+}) pair simulation and is a consequence of the low number of countable events.

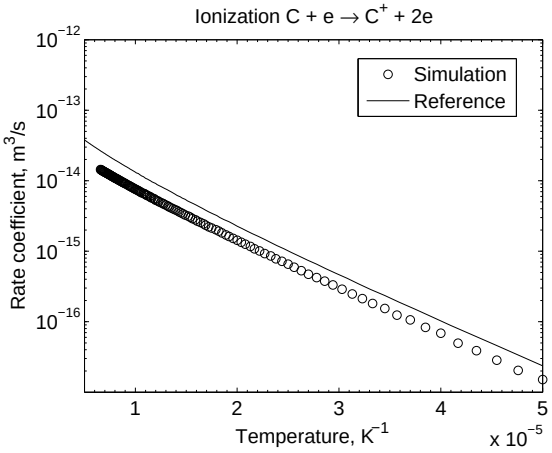

Figure 3. The simulated ionization rate coefficient for (e, C) pairs in comparison with the reference.[26]

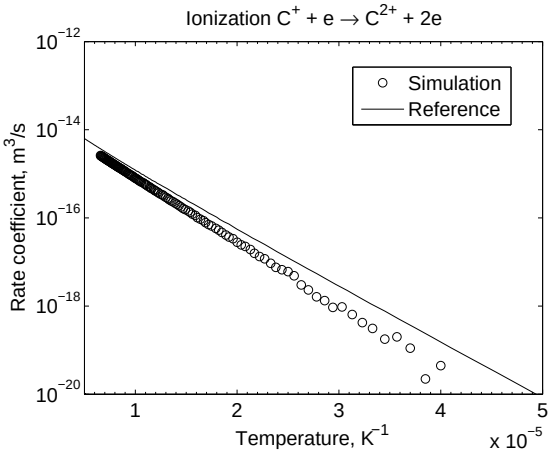

Figure 4. The simulated ionization rate coefficient for (e, C^{+}) pairs in comparison with the reference.[26]

3. Recombination

The recombination rate coefficients for the (e, C^{+}) and (e, C^{2+}) particle pairs are given in Fig. 5 and Fig. 6. The comparison with the numerical reference Eq. (23) shows a good agreement. Due to low reaction probabilities of these processes only a small number of events could be registered. The *Detailed Balancing* principle implies increasing recombination cross sections with increasing ionization cross sections which is here the case for high temperatures. The ionization cross section for C^{+} ions is smaller than for C atoms. Therefore, for (e, C^{2+}) pairs less recombination events were counted than for (e, C^{+}) pairs. No counts were registered for (e, C^{3+}) pairs (not presented here). Due to the low number of events no relative deviation is provided.

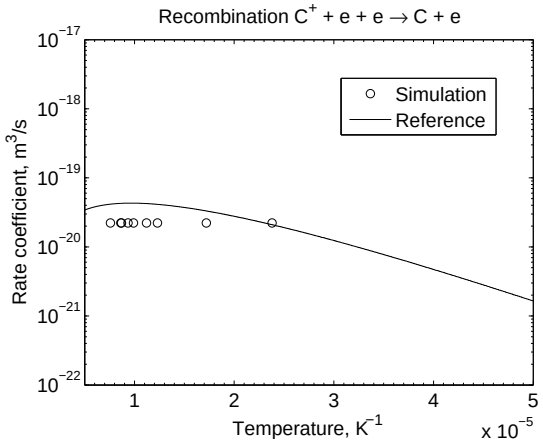

Figure 5. The simulated recombination rate coefficient for (e, C^+) pairs in comparison with the reference (Eq. (23)).

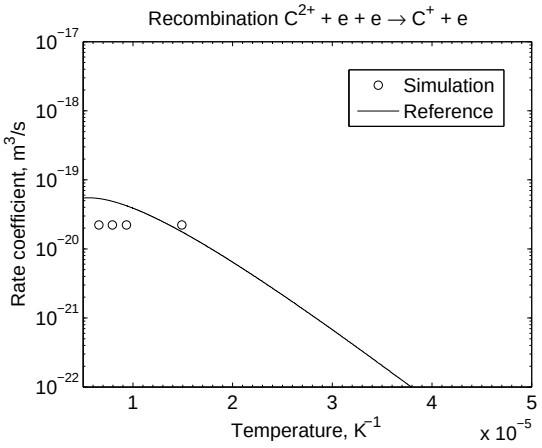

Figure 6. The simulated recombination rate coefficient for (e, C^{2+}) pairs in comparison with the reference (Eq. (23)).

4. Excitation

In case of electron excitation processes the focus was on excitation of ground state atoms, see Fig. 7. A very good agreement in the complete temperature range could be achieved between simulated rate coefficient and the reference. The maximum relative deviation equals 25.7% at T_{max} and approaches 2.8% at T_{min}.

However, the excitation verification in case of ionized ground state species failed presumably due to the difficulties in modeling the Coulomb collision cross section accurately. This concerns all C^{n+} species.

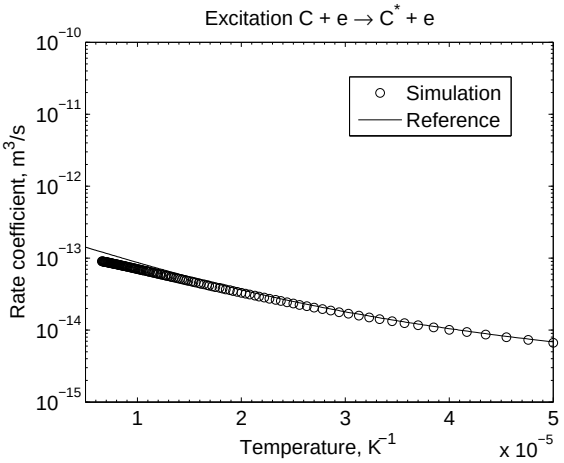

Figure 7. The simulated excitation rate coefficient for (e, C) pairs in comparison with the reference (Eq. (23)).

5. De-excitation

The deviation of the simulated de-excitation rate coefficient is in comparison with the reference remarkably high although ionization, recombination, and excitation verification suggests that the implementation of the model and data algorithms should be correct. Two potential error sources were identified:

- The cause could be found in the initialization of the heavy particles in DSMC. Comparative simulations were performed under variation of the excitation initialization - no excitation (i.e. all in ground state), Boltzmann distribution, and all heavy particles in a first state excitation. Consequently, different rate coefficients were obtained for all excited species. However, in the computation of the numerical reference Eq. (23) *all* defined states and transitions are considered. In the initialization not all states are occupied, thus a deviation would be not surprising. A supporting indication is the fact that the

numerically integrated reference is larger than the simulated rate coefficient. This problem can be solved by adapting the integration routine in a way that only those states and transitions are taken into account which are initialized in the particle simulation.

- Even more probable is the scenario related to the numerical tool which generates the numerical reference. Physically, the integrator should couple two distribution functions: the continuous electron velocity distribution function and the discrete Boltzmann distribution function. However, in the current version only the continuous electron velocity distribution function is considered such that excitation distribution is neglected.

III. MCCC Model, Verification, and Discussion

As mentioned before, the Coulomb interaction is based on a long range interaction which cannot be treated with standard DSMC. Otherwise, one would need to define a Coulomb cross section whose integral value diverges. The traditional integration simplifications leading to a finite value (limiting the electrostatic interaction range to λ_D or introducing a cut-off scattering angle χ_{cut}) are basically arbitrary.[27]

A. Brief Introduction to Basic Theory

A way out of this dilemma was provided by Nanbu.[12,28] His Monte Carlo Coulomb Collision (MCCC) method is based on the theory of cumulative scattering. Here, we give only a very brief introduction, for further details please refer to the given references. Resolving λ_D implies $P_c > 1$ for all pairs of charged particles as every charge in the Debye sphere by definition interacts with every other charge in that sphere. This prohibits a binary treatment modeling. Nanbu found a simple expression for the probability density distribution $F(\chi_N)$ of the cumulative scattering angle χ_N after N scattering processes,

$$F(\chi_N) = 2\pi \sin\chi_N \; f(\chi_N). \tag{24}$$

Starting point was the clarification of the coordinate transformation process due to scattering. Given the transformation matrix he simulated N single scattering processes on very small time scales and traced the cumulated scattering angle χ_N. It's distribution as a function of time was approximated quite well by an exponential approach which together with the normalization condition

$$2\pi \int_0^\pi f(\chi_N) \sin\chi_N \mathrm{d}\chi_N = 1 \tag{25}$$

leads to

$$f(\chi_N) = \frac{A}{4\pi \sinh A} \exp\left(A\cos\chi_N\right) \tag{26}$$

where A is a function to be defined. Additionally, Nanbu traced the expectation value $\left\langle \sin^2 \frac{\chi_N}{2} \right\rangle$ as a function of N which can be approximated very good by

$$\left\langle \sin^2 \frac{\chi_N}{2} \right\rangle = \frac{1}{2}\left[1 - \exp\left(-\tau\right)\right]. \tag{27}$$

The averaging process

$$2\pi \int_0^\pi f(\chi_N) \sin^2 \frac{\chi_N}{2} \sin\chi_N \mathrm{d}\chi_N = \frac{1}{2}\left[1 - \exp\left(-\tau\right)\right] \tag{28}$$

in combination with (26) allows to identify a relation for the unknown A in Eq. (26):

$$\coth A - A^{-1} = \exp\left(-\tau\right). \tag{29}$$

System parameters like time step size $\triangle t$, particle densities n, charges q and others are hidden in the so-called isotropy parameter τ:

$$\tau = \frac{\ln\Lambda}{4\pi} \left(\frac{Z_\alpha Z_\beta e^2}{\varepsilon_0 m_r}\right)^2 n_\beta g^{-3} \triangle t. \tag{30}$$

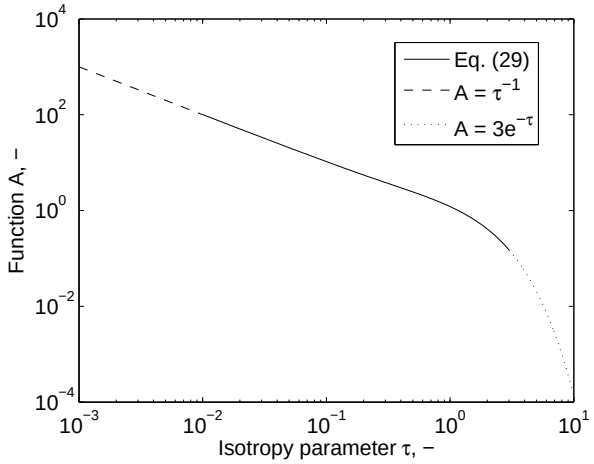

Figure 8. A **as a function of different** τ**.**

Equation (29) cannot be solved analytically but numerically. Nanbu[12] provides values for all τ and A which are not covered by the following relation:

$$A = \begin{cases} \tau^{-1} & \text{for } \tau < 0.01, \\ 3e^{-\tau} & \text{for } \tau > 3. \end{cases} \tag{31}$$

See Fig. 8 for a visual presentation of $A(\tau)$. Given that, a sample of χ_N can be obtained from

$$\cos\chi_N = A^{-1} \ln\left(e^{-A} + 2R\sinh A\right) \tag{32}$$

where the main input parameter is an equally distributed random number $R \in [0,1]$. Once χ_N is known, post-collisional particle velocities (marked with ($'$)) as a result of Coulmb scattering can be derived:

$$\vec{v}'_\alpha = \vec{v}_\alpha - \frac{m_\beta}{m_\alpha + m_\beta}[\vec{g}(1-\cos\chi_N) + \vec{h}\sin\chi_N] \tag{33}$$

$$\vec{v}'_\beta = \vec{v}_\beta + \frac{m_\alpha}{m_\alpha + m_\beta}[\vec{g}(1-\cos\chi_N) + \vec{h}\sin\chi_N]. \tag{34}$$

In cartesian coordinates one has then

$$h_x = g_\perp \cos\varepsilon \tag{35}$$

$$h_y = -(g_x g_y \cos\varepsilon + g g_z \sin\varepsilon)/g_\perp \tag{36}$$

$$h_z = -(g_x g_z \cos\varepsilon - g g_y \sin\varepsilon)/g_\perp \tag{37}$$

$$g_\perp = (g_y^2 + g_z^2)^{1/2} \tag{38}$$

with ε representing the azimuthal (and isotropic) scattering angle. A verification of the implementation is presented in the following.

B. Verification and Discussion

The verification of the MCCC implementation is based on the analytical solutions[29] of the drift and variance evolution over time for the following test cases: an electron beam is shot into an ion cloud, and an electron beam is shot into an electron cloud. For the first test case long term solutions are known due to the fact that electron and ion masses are so different such that $m_e/m_i \approx 0$ can be assumed. For the second test case only short term solutions are available. For both test cases the reservoir conditions are summarized in the Appendix, see Table 3 and Table 4.

1. Electron Beam Shot Into Ion Cloud

Following Trubnikov,[29] the characteristic relaxation frequency $\nu^{(\alpha,\beta)}$ can be obtained from

$$\nu^{(\alpha,\beta)} = \frac{8\pi\sqrt{2m_\alpha}\varepsilon_0(E_{x,0})^{3/2}}{n_\beta\left(Z_\alpha Z_\beta e^2\right)^2}\ln\Lambda_{\alpha\beta} \tag{39}$$

where $E_{x,0}$ is the initial electron beam energy. With $\alpha = e$ and $\beta = i$ the electron drift velocity in x-direction $\hat{v}_\parallel(t) = \hat{v}_x(t)$ evolves over time according to

$$\langle\hat{v}_\parallel(t)\rangle = \exp\Big\{-\nu_{(e,i)}\,(t-t_0)\Big\}\,\hat{v}_{x,0}. \tag{40}$$

Due to normalization with respect to the initial velocity, $\hat{v}_{x,0} = \hat{v}_x(t = t_0) = 1$. For the variance of each component one gets

$$\begin{aligned}\langle\hat{v}_\parallel^2(t)\rangle = \frac{1}{3}\Big[1 - \exp\Big\{-3\,\nu^{(e,i)}(t-t_0)\Big\}\Big] \\ + \Big[\exp\Big\{-3\,\nu^{(e,i)}(t-t_0)\Big\} - \exp\Big\{-2\,\nu^{(e,i)}(t-t_0)\Big\}\Big]\,\hat{v}_{x,0}^2\end{aligned} \tag{41}$$

and

$$\langle\hat{v}_y^2(t)\rangle = \langle\hat{v}_z^2(t)\rangle = \frac{1}{3}\Big[1 - \exp\Big\{-3\,\nu^{(e,i)}(t-t_0)\Big\}\Big]. \tag{42}$$

In all cases the equilibrium solution equals 1/3. Since $T_{e,0} << T_{i,0}$ collisional processes lead to an increase of ion temperature. For realization of $m_e/m_i \to 0$ the electron temperature was set constant. In both test cases the electron beam is supposed to be as mono-energetic as possible such that initial temperature was set to be very low.

The results are depicted in Fig. 9 and Fig. 10 where the time is normalized according to $\hat{t} = t \cdot \nu^{(e,i)}$. The electron drift loses successively kinetic energy which is transferred into thermal energy. Statistic effects can be observed at low drift velocities, i.e. at larger times where the drift scatters around the reference. The increase of scattering can be explained by an decreasing signal-to-noise ratio. With increasing time thermal velocity components increase as observable in Fig. 10. The temperature increase shows a significant difference in the dynamics of the longitudinal and transversal degree(s) of freedom. As expected, the transversal component reaches the (correct) equilibrium state faster than the longitudinal one.

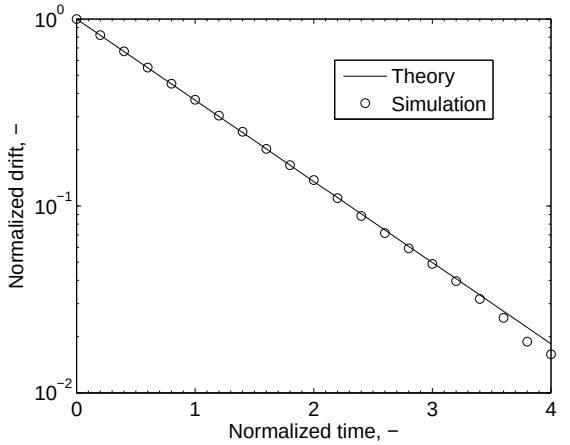

Figure 9. Temporal long term evolution of the theoretical (see Eq. (40)) and numerical drift.

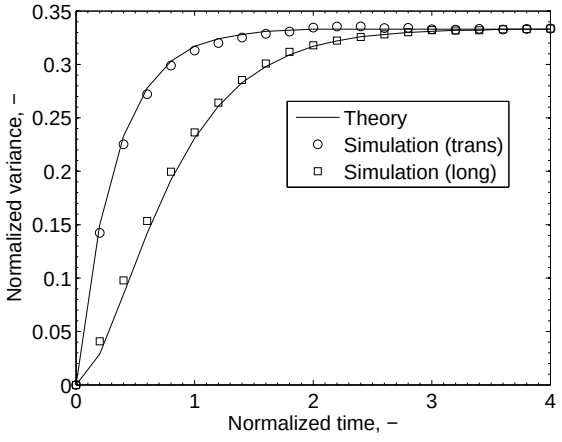

Figure 10. Temporal long term evolution of theoretical (see Eq. (42)) and numerical variances of longitudinal and transversal modes.

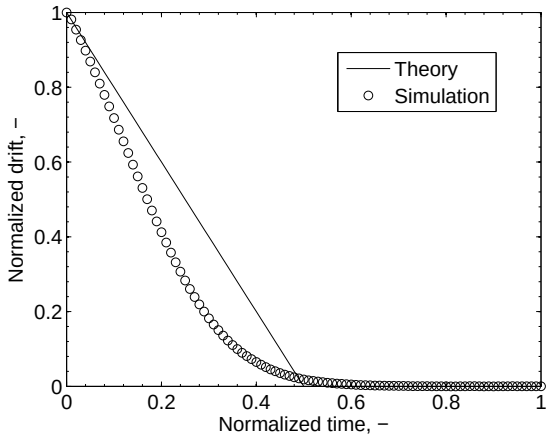

Figure 11. Temporal evolution of electron beam drift velocity, compared with theoretical short term solution (see Eq. (43)).

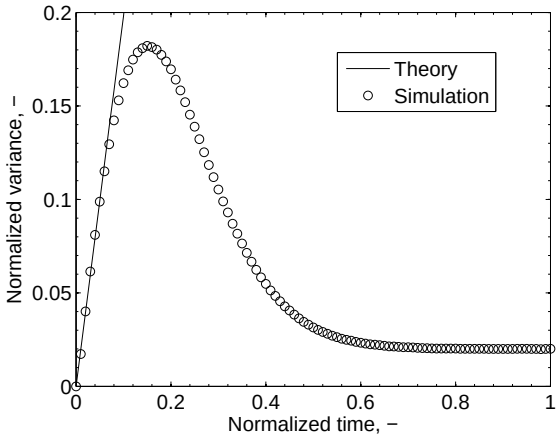

Figure 12. Temporal evolution of electron beam variance, compared with theoretical short term solution (see Eq. (44)).

2. Electron Beam Shot Into Electron Cloud

Another but similar configuration is used for additional verification of the MCCC implementation. Now, an electron beam is shot into an electron cloud in order to resolve (e, e) scattering. Due to the mass similarity the simplification $m_e/m_i \to 0$ cannot be made such that only short term solutions of drift and variance evolution exist:[29]

$$\langle \hat{v}_{\parallel} \rangle = 1 - 2\hat{t}, \tag{43}$$

$$\langle \hat{v}_{\perp}^2 \rangle = (2 - \eta_{\alpha\beta}^{-1})\hat{t}. \tag{44}$$

Here, $\eta_{\alpha\beta} = E_{x,0}/k_B T_\beta = 50$. In general, a validity range of both short term solutions cannot be given. However, following Nanbu[12] equilibrium state is characterized by $\langle \hat{v}_{\perp}^2 \rangle = \eta_{\alpha\beta}^{-1} = 0.02$, compare Fig. 12. In Fig. 11 one can see that thermalization proceeds much faster with respect to the (e, i) case.

IV. Conclusions

A large and unique Carbon related cross section data base was implemented in a DSMC code according to a newly developed and very flexible collision and reaction scheme. The modeling concerns the elastic collisions between electrons and neutrals (including polarization), the electron impact ionization and corresponding recombination, and the electron impact excitation and corresponding de-excitation. For the sake of accuracy, the cross section of the concurring radiative recombination process is also considered. Elastic scattering between electrons and ions is treated on basis of a simplified model for the Coulomb cross section. Ground state atom excitation and three-body recombination were successfully verified. Although the ionization rate coefficients reaches up to approx. 50% relative deviation from the reference we consider the implementation as verified. The numerical reference was meant to be applied only in cases where no references were found in the literature which was not the case for the presented ionization processes. However, cross section and reference were taken from different sources such that a mismatch is not surprising. Moreover, keep in mind that the whole approach regarding the probability evaluation in DSMC does not contain a single element which makes us expect that the (equilibrium) rate coefficient would be reproduced under equilibrium conditions.

From the presented results it is concluded that the discussed model approach is generally feasible for providing a DSMC based collision scheme of high fidelity without making use of equilibrium related quantities like viscosity or diffusion. However, the trade-off is the need of cross section data of correspondingly high accuracy. Although the expression for the (three-body) recombination cross section contains the electron temperature, it is considered as a negligible violation of the desired consistency.

For electron-ion pairs the highest number of cross sections is needed. Thus, the probability computation is generally most erroneous. However, the successful verification of the collisional recombination process shows

that, to a certain degree, the uncertainty of the applied cross section models is smeared due to the cross section summation. Therefore, it is concluded that the quality of a cross section model (and the corresponding data set) can be studied in depth by simulating pair dependent particle interactions in reasonably chosen temperature ranges on basis of a purely energy dependent model as the one presented here.

Several DSMC related problems were identified which need to be considered in future works:

- The major problem concerns the Coulomb cross section. In a first step the accuracy of the formulation should be improved. Therefore, it appears useful to implement other species with high fidelity cross section data like Argon which are even more accurate than the presented Carbon based data set. This could be a starting point for the quantitative determination of a Coulomb collision cross section usable in DSMC schemes. Consequently, a more accurate Coulomb collision cross section model would not only improve some of the already verified interactions, but would also lead to the verification of further species like C^{n+} ions especially with respect to excitation processes.
- The verification of collisional de-excitation processes failed, two potential reasons were discussed and need attention in future activities.
- The ionization verification should be repeated on basis of self-generated reference data.

Additionally, a MCCC model for the kinetic treatment of Coulomb collisions was implemented and successfully verified. In Nanbu's original publication for both scenarios a comparison with short term solutions only was given. Here, we provided a comparison with the long term solution for the (e, i) case which significantly improves the verification quality. However, by definition every numerical tool can be verified only within the frame of the assumption made such that future activities should contain further verifications. Possible test case scenarios are:

- Electron beam shot into a plasma cloud investigating beam drift and variance.
- Relaxation of a non-equilibrium function in an electron gas on basis of (e, e) collisions.
- Relaxation of an initial distribution function of an electron flow in an ion gas.
- Relaxation of non-equilibrium distribution functions in a plasma.
- Evolution of electron drift velocity in an oscillating electric field.

For these problems reference solutions are available. However, further verification of the MCCC appears not to be of highest priority.

Appendix

Table 1. Assignment of particle type and interaction number.

Type	A	M	e	I	M^+	A^*	I^*	M^*	M^{*+}	...
InterID	1	2	4	10	20	40	100	200	400	...

Table 2. Main parameters for the DSMC model verification. T_h is the heavy particle temperature, N is the total particle number.

$n,\ m^{-3}$	$\triangle t,\ s$	$N,\ -$	$T_h,\ kK$	$T_e,\ kK$
$3.6 \cdot 10^{21}$	10^{-10}	$3.6 \cdot 10^5$	2	$20 - 200$

Table 3. Main parameters for the verification of the MCCC solver - electron beam shot into ion cloud.

$n,\ m^{-3}$	$\Psi_{e,Ar^+},\ -$	$\triangle t,\ s$	$T_e,\ K$	$E_{x,0},\ eV$
$2 \cdot 10^{18}$	0.5	$2.79 \cdot 10^{-7}$	1	30

Table 4. Main parameters for the verification of the MCCC solver - electron beam shot into an electron cloud. Index E is used for the background (i.e. cloud) electron species.

$\triangle t,\ s$	$T_E,\ eV$	$E_{x,0},\ eV$
$3.04 \cdot 10^{-7}$	2	100

Acknowledgments

The authors gratefully acknowledge the Landesstiftung Baden-Württemberg for the initial funding as well as the DFG for the financial support.

References

[1]Nawaz, A., *Entwicklung und Charakterisierung eines gepulsten instationäaren MPD Triebwerks als Primärantrieb für Weltraumsonden*, Dissertation, Institut fr Raumfahrtsysteme, Universitt Stuttgart, 2009.

[2]Burnett, D., "The distribution of melocular velocities and the mean motion in a non-uniform gas," *Proc. Lond. Math. Soc.*, Vol. 40, 1935, pp. 382–435.

[3]Grad, H., "On the kinetic theory of rarefied gases," *Commun. Pure Appl. Math.*, Vol. 2, 1949, pp. 331–407.

[4]Reese, J. M., Gallis, M. A., and Lockerby, D. A., "New directions in fluid dynamics: non-equilibrium aerodynamic and microsystem flows," *Phil. Trans. R. Soc. Lond.*, Vol. A, No. 361, 2003, pp. 2967–2988.

[5]Boyd, I. D., Keidar, M., and McKeon, W., "Modeling of a Pulsed Plasma Thruster from Plasma Generation to Plume Far Field," *Journal of Propulsion and Power*, Vol. 37, No. 3, 2000, pp. 399–407.

[6]Gatsonis, N. A. and Yin, X., "Hybrid (Particle-Fluid) Modeling of Pulsed Plasma Thruster Plumes," *Journal of Propulsion and Power*, Vol. 17, No. 5, 2001, pp. 945–958.

[7]Keidar, M., Boyd, I. D., Antonsen, E., and Spanjers, G. G., "Electromagnetic Effects in the Near-Field Plume Exhaust of a Micro-Pulsed-Plasma Thruster," *Journal of Propulsion and Power*, Vol. 20, No. 6, Nov. 2004, pp. 961–969.

[8]Cercignani, C., *Mathematical Methods in Kinetic Theory, Sec. Ed.*, Plenum Press, New York and London, 1990.

[9]Cercignani, C., Illner, R., and Pulvirenti, M., *The Mathematical Theory of Dilute Gases*, Applied Mathematical Sciences 106, Springer Verlag, 1994.

[10]Rjasanow, S. and Wagner, W., *Stochastic Numerics for the Boltzmann Equation*, Springer-Verlag Berlin Heidelberg, 2005.

[11]Neudorfer, J., Stindl, T., Schneider, R., Roller, S., Munz, C. D., and Auweter-Kurtz, M., "Three-dimensional Particle-In-Cell simulation of a Pulsed Plasma Thruster: Modelling and Challenges," IEPC-2011-116, to be presented at the 32nd International Electric Propulsion Conference, Würzburg, Germany, Sep 11-15 2011.

[12]Nanbu, K., "Theory of cumulative small-angle collisions in plasmas," *Phys. Rev. E*, Vol. 55, 1997, pp. 4642–4652.

[13]D'Andrea, D., *Modelling of Intra- and Inter Species Charged Particle Collisions for Flow Simulation in Pulsed Plasma Thrusters*, Dissertation, Institut für Aerodynamik und Gasdynamik, Universität Stuttgart, 2008.

[14]Bird, G., *Molecular Gas Dynamics and the Direct Simulation of Gas Flows*, Clarendon Press, Oxford, 1994.

[15]Hassan, H. A. and Hash, D. B., "A generalized hard-sphere model for Monte Carlo simulation," *Phys. Fluids A*, Vol. 5, No. 3, 1993, pp. 738–744.

[16]Baganoff, D. and McDonald, J. D., "A Collision-Selection Rule for a Particle Simulation Method suited to Vector Computers," *Phys. Fluids A*, Vol. 2(7), 1990, pp. 1248–1259.

[17]Chernyi, G. G., Losev, S. A., Macheret, S. O., and Potapkin, B. V., *Physical and Chemical Processes in Gas Dynamics: Cross Sections and Rate Constants, Volume 1*, AIAA - Progress in Astronautics and Aeronautics, 181 Alexander Bell Drive, Suite 500, Reston, VA 20191-4344, USA, 2002.

[18]Gupta, A., Bhattacharya, A. K., and Mukherjee, P. K., "Coupled Hartree Fock Calculation of Static Dipole Polarizabilities and Shielding Factors of Open Shell Systems," *Int. J. Quant. Chem.*, Vol. VIII, 1974, pp. 97–105.

[19]Suno, H. and Kato, T., "Cross section database for carbon atoms and ions: Electron impact ionization, excitation, and charge exchange in collisions with hydrogen atoms," *Atomic Data and Nuclear Data Tables*, Vol. 92, No. 4, 2006, pp. 407–455.

[20]Burke, P. G., "The Convergence of the Close Coupling Expansion," *Proceedings of the Physical Society*, Vol. 82, 1963, pp. 443–445.

[21]Burke, P. G. and Joachain, C. J., *Theory of Electron-Atom Collisions: Part 1: Potential Scattering*, Plenum Press, 1995.

[22]Bogaerts, A., Gijbels, R., and Vlcek, J., "Collisional-radiative model for an argon glow discharge," *J. Appl. Phys.*, Vol. 84, No. 1, 1998, pp. 121–136.

[23]van de Sanden, M. C. M., Schram, P. P. J. M., Peeters, A. G., van der Mullen, J. A. M., and Kroesen, G. M. W., "Thermodynamic generalization of the Saha equation for a two-temperature plasma," *Phys. Rev. A*, Vol. 40, No. 9, 1989, pp. 5273–5276.

[24]Seaton, M. J., Zeippen, C. J., Tully, J. A., Pradhan, A. K., Mendoza, C., Hibbert, A., and Berrington, K. A., "The Opacity Project - Computation of Atomic Data," *Rev. Mexicana Astron. Astrof.*, Vol. 23, 1992, pp. 19–43.

[25]Jahn, R., *Physics of Electric Propulsion*, McGraw-Hill, New York, 1968.

[26]Voronov, G. S., "A Practical Fit Formula for Ionization Rate Coefficients of Atoms and Ions by Electron Impact: $Z = 1 - 28$," *Atomic Data and Nuclear Data Tables*, Vol. 65, No. 1, 1997, pp. 1–35.

[27]Chang, Y., "The concept of collision strength and a unified kinetic calculation for hard-sphere interactions and inverse square force law interactions," *Phys. Plasmas*, Vol. 10, No. 12, 2003, pp. 4645–4660.

[28]Bobylev, A. V. and Nanbu, K., "Theory of collision algorithms for gases and plasmas based on the Boltzmann equation and Landau-Fokker-Planck equation," *Phys. Rev. E*, Vol. 61, 2000, pp. 4576–4586.

[29]Trubnikov, B. A., *Particle interactions in a fully ionized plasma*, Reviews of Plasma Physics, Consultants Bureau, New York, 1965.